12-5-2018

Measurement of the $\gamma^*\gamma^* \rightarrow \eta'$ Transition Form Factor

J.P. Lees

V. Poireau

V. Tisserand

E. Grauges

A. Palano

See next page for additional authors

Publication Info

Published in *Physical Review D*, Volume 98, Issue 11, 2018.
Published by the American Physical Society under the terms of the Creative Commons Attribution 4.0 International license. Further distribution of this work must maintain attribution to the author(s) and the published article's title, journal citation, and DOI. Funded by SCOAP^3.

Author(s)

J.P. Lees, V. Poireau, V. Tisserand, E. Grauges, A. Palano, G. Eigen, D. N. Brown, Yu G. Kolomensky, M. Fritsch, H. Koch, T. Schroeder, C. Hearty, T. S. Mattison, J. A. McKenna, R. Y. So, V. E. Blinov, A. R. Buzykaev, V. P. Druzhinin, V. B. Golubev, Milind Purohit, and Et. Al.

PHYSICAL REVIEW D **98,** 112002 (2018)

Measurement of the $\gamma^*\gamma^* \to \eta'$ transition form factor

J. P. Lees,[1] V. Poireau,[1] V. Tisserand,[1] E. Grauges,[2] A. Palano,[3] G. Eigen,[4] D. N. Brown,[5] Yu. G. Kolomensky,[5] M. Fritsch,[6] H. Koch,[6] T. Schroeder,[6] C. Hearty,[7a,7b] T. S. Mattison,[7b] J. A. McKenna,[7b] R. Y. So,[7b] V. E. Blinov,[8a,8b,8c] A. R. Buzykaev,[8a] V. P. Druzhinin,[8a,8b] V. B. Golubev,[8a,8b] E. A. Kozyrev,[8a,8b] E. A. Kravchenko,[8a,8b] A. P. Onuchin,[8a,8b,8c] S. I. Serednyakov,[8a,8b] Yu. I. Skovpen,[8a,8b] E. P. Solodov,[8a,8b] K. Yu. Todyshev,[8a,8b] A. J. Lankford,[9] J. W. Gary,[10] O. Long,[10] A. M. Eisner,[11] W. S. Lockman,[11] W. Panduro Vazquez,[11] D. S. Chao,[12] C. H. Cheng,[12] B. Echenard,[12] K. T. Flood,[12] D. G. Hitlin,[12] J. Kim,[12] Y. Li,[12] T. S. Miyashita,[12] P. Ongmongkolkul,[12] F. C. Porter,[12] M. Röhrken,[12] Z. Huard,[13] B. T. Meadows,[13] B. G. Pushpawela,[13] M. D. Sokoloff,[13] L. Sun,[13,†] J. G. Smith,[14] S. R. Wagner,[14] D. Bernard,[15] M. Verderi,[15] D. Bettoni,[16a] C. Bozzi,[16a] R. Calabrese,[16a,16b] G. Cibinetto,[16a,16b] E. Fioravanti,[16a,16b] I. Garzia,[16a,16b] E. Luppi,[16a,16b] V. Santoro,[16a] A. Calcaterra,[17] R. de Sangro,[17] G. Finocchiaro,[17] S. Martellotti,[17] P. Patteri,[17] I. M. Peruzzi,[17] M. Piccolo,[17] M. Rotondo,[17] A. Zallo,[17] S. Passaggio,[18] C. Patrignani,[18,‡] H. M. Lacker,[19] B. Bhuyan,[20] U. Mallik,[21] C. Chen,[22] J. Cochran,[22] S. Prell,[22] A. V. Gritsan,[23] N. Arnaud,[24] M. Davier,[24] F. Le Diberder,[24] A. M. Lutz,[24] G. Wormser,[24] D. J. Lange,[25] D. M. Wright,[25] J. P. Coleman,[26] E. Gabathuler,[26,*] D. E. Hutchcroft,[26] D. J. Payne,[26] C. Touramanis,[26] A. J. Bevan,[27] F. Di Lodovico,[27] R. Sacco,[27] G. Cowan,[28] Sw. Banerjee,[29] D. N. Brown,[29] C. L. Davis,[29] A. G. Denig,[30] W. Gradl,[30] K. Griessinger,[30] A. Hafner,[30] K. R. Schubert,[30] R. J. Barlow,[31,§] G. D. Lafferty,[31] R. Cenci,[32] A. Jawahery,[32] D. A. Roberts,[32] R. Cowan,[33] S. H. Robertson,[34a,34b] R. M. Seddon,[34b] B. Dey,[35a] N. Neri,[35a] F. Palombo,[35a,35b] R. Cheaib,[36] L. Cremaldi,[36] R. Godang,[36,¶] D. J. Summers,[36] P. Taras,[37] G. De Nardo,[38] C. Sciacca,[38] G. Raven,[39] C. P. Jessop,[40] J. M. LoSecco,[40] K. Honscheid,[41] R. Kass,[41] A. Gaz,[42a] M. Margoni,[42a,42b] M. Posocco,[42a] G. Simi,[42a,42b] F. Simonetto,[42a,42b] R. Stroili,[42a,42b] S. Akar,[43] E. Ben-Haim,[43] M. Bomben,[43] G. R. Bonneaud,[43] G. Calderini,[43] J. Chauveau,[43] G. Marchiori,[43] J. Ocariz,[43] M. Biasini,[44a,44b] E. Manoni,[44a] A. Rossi,[44a] G. Batignani,[45a,45b] S. Bettarini,[45a,45b] M. Carpinelli,[45a,45b,**] G. Casarosa,[45a,45b] M. Chrzaszcz,[45a] F. Forti,[45a,45b] M. A. Giorgi,[45a,45b] A. Lusiani,[45a,45c] B. Oberhof,[45a,45b] E. Paoloni,[45a,45b] M. Rama,[45a] G. Rizzo,[45a,45b] J. J. Walsh,[45a] L. Zani,[45a,45b] A. J. S. Smith,[46] F. Anulli,[47a] R. Faccini,[47a,47b] F. Ferrarotto,[47a] F. Ferroni,[47a,47b] A. Pilloni,[47a,47b] G. Piredda,[47a,*] C. Bünger,[48] S. Dittrich,[48] O. Grünberg,[48] M. Heß,[48] T. Leddig,[48] C. Voß,[48] R. Waldi,[48] T. Adye,[49] F. F. Wilson,[49] S. Emery,[50] G. Vasseur,[50] D. Aston,[51] C. Cartaro,[51] M. R. Convery,[51] J. Dorfan,[51] W. Dunwoodie,[51] M. Ebert,[51] R. C. Field,[51] B. G. Fulsom,[51] M. T. Graham,[51] C. Hast,[51] W. R. Innes,[51,*] P. Kim,[51] D. W. G. S. Leith,[51] S. Luitz,[51] D. B. MacFarlane,[51] D. R. Muller,[51] H. Neal,[51] B. N. Ratcliff,[51] A. Roodman,[51] M. K. Sullivan,[51] J. Va'vra,[51] W. J. Wisniewski,[51] M. V. Purohit,[52] J. R. Wilson,[52] A. Randle-Conde,[53] S. J. Sekula,[53] H. Ahmed,[54] M. Bellis,[55] P. R. Burchat,[55] E. M. T. Puccio,[55] M. S. Alam,[56] J. A. Ernst,[56] R. Gorodeisky,[57] N. Guttman,[57] D. R. Peimer,[57] A. Soffer,[57] S. M. Spanier,[58] J. L. Ritchie,[59] R. F. Schwitters,[59] J. M. Izen,[60] X. C. Lou,[60] F. Bianchi,[61a,61b] F. De Mori,[61a,61b] A. Filippi,[61a] D. Gamba,[61a,61b] L. Lanceri,[62] L. Vitale,[62] F. Martinez-Vidal,[63] A. Oyanguren,[63] J. Albert,[64b] A. Beaulieu,[64b] F. U. Bernlochner,[64b] G. J. King,[64b] R. Kowalewski,[64b] T. Lueck,[64b] I. M. Nugent,[64b] J. M. Roney,[64b] R. J. Sobie,[64a,64b] N. Tasneem,[64b] T. J. Gershon,[65] P. F. Harrison,[65] T. E. Latham,[65] R. Prepost,[66] and S. L. Wu[66]

(*BaBar* Collaboration)

[1]*Laboratoire d'Annecy-le-Vieux de Physique des Particules (LAPP), Université de Savoie, CNRS/IN2P3,*
F-74941 Annecy-Le-Vieux, France
[2]*Universitat de Barcelona, Facultat de Fisica, Departament ECM, E-08028 Barcelona, Spain*
[3]*INFN Sezione di Bari and Dipartimento di Fisica, Università di Bari, I-70126 Bari, Italy*
[4]*University of Bergen, Institute of Physics, N-5007 Bergen, Norway*
[5]*Lawrence Berkeley National Laboratory and University of California, Berkeley, California 94720, USA*
[6]*Ruhr Universität Bochum, Institut für Experimentalphysik 1, D-44780 Bochum, Germany*
[7a]*Institute of Particle Physics, Vancouver, V6T 1Z1 British Columbia, Canada*
[7b]*University of British Columbia, Vancouver, V6T 1Z1 British Columbia, Canada*
[8a]*Budker Institute of Nuclear Physics SB RAS, Novosibirsk 630090, Russia*
[8b]*Russia Novosibirsk State University, Novosibirsk 630090, Russia*
[8c]*Novosibirsk State Technical University, Novosibirsk 630092, Russia*
[9]*University of California at Irvine, Irvine, California 92697, USA*
[10]*University of California at Riverside, Riverside, California 92521, USA*
[11]*University of California at Santa Cruz, Institute for Particle Physics, Santa Cruz, California 95064, USA*
[12]*California Institute of Technology, Pasadena, California 91125, USA*
[13]*University of Cincinnati, Cincinnati, Ohio 45221, USA*
[14]*University of Colorado, Boulder, Colorado 80309, USA*
[15]*Laboratoire Leprince-Ringuet, Ecole Polytechnique, CNRS/IN2P3, F-91128 Palaiseau, France*

2470-0010/2018/98(11)/112002(11) Published by the American Physical Society

[16a]*INFN Sezione di Ferrara, I-44122 Ferrara, Italy*
[16b]*Dipartimento di Fisica e Scienze della Terra, Università di Ferrara, I-44122 Ferrara, Italy*
[17]*INFN Laboratori Nazionali di Frascati, I-00044 Frascati, Italy*
[18]*INFN Sezione di Genova, I-16146 Genova, Italy*
[19]*Humboldt-Universität zu Berlin, Institut für Physik, D-12489 Berlin, Germany*
[20]*Indian Institute of Technology Guwahati, Guwahati, 781 039 Assam, India*
[21]*University of Iowa, Iowa City, Iowa 52242, USA*
[22]*Iowa State University, Ames, Iowa 50011, USA*
[23]*Johns Hopkins University, Baltimore, Maryland 21218, USA*
[24]*Laboratoire de l'Accélérateur Linéaire, IN2P3/CNRS et Université Paris-Sud 11, Centre Scientifique d'Orsay, F-91898 Orsay Cedex, France*
[25]*Lawrence Livermore National Laboratory, Livermore, California 94550, USA*
[26]*University of Liverpool, Liverpool L69 7ZE, United Kingdom*
[27]*Queen Mary, University of London, London E1 4NS, United Kingdom*
[28]*University of London, Royal Holloway and Bedford New College, Egham, Surrey TW20 0EX, United Kingdom*
[29]*University of Louisville, Louisville, Kentucky 40292, USA*
[30]*Johannes Gutenberg-Universität Mainz, Institut für Kernphysik, D-55099 Mainz, Germany*
[31]*University of Manchester, Manchester M13 9PL, United Kingdom*
[32]*University of Maryland, College Park, Maryland 20742, USA*
[33]*Massachusetts Institute of Technology, Laboratory for Nuclear Science, Cambridge, Massachusetts 02139, USA*
[34a]*Institute of Particle Physics, Montréal, Québec H3A 2T8, Canada*
[34b]*McGill University, Montréal, Québec H3A 2T8, Canada*
[35a]*INFN Sezione di Milano, I-20133 Milano, Italy*
[35b]*Dipartimento di Fisica, Università di Milano, I-20133 Milano, Italy*
[36]*University of Mississippi, University, Mississippi 38677, USA*
[37]*Université de Montréal, Physique des Particules, Montréal, H3C 3J7 Québec, Canada*
[38]*INFN Sezione di Napoli and Dipartimento di Scienze Fisiche, Università di Napoli Federico II, I-80126 Napoli, Italy*
[39]*NIKHEF, National Institute for Nuclear Physics and High Energy Physics, NL-1009 DB Amsterdam, Netherlands*
[40]*University of Notre Dame, Notre Dame, Indiana 46556, USA*
[41]*Ohio State University, Columbus, Ohio 43210, USA*
[42a]*INFN Sezione di Padova, I-35131 Padova, Italy*
[42b]*Dipartimento di Fisica, Università di Padova, I-35131 Padova, Italy*
[43]*Laboratoire de Physique Nucléaire et de Hautes Energies, IN2P3/CNRS, Université Pierre et Marie Curie-Paris6, Université Denis Diderot-Paris7, F-75252 Paris, France*
[44a]*INFN Sezione di Perugia, I-06123 Perugia, Italy*
[44b]*Dipartimento di Fisica, Università di Perugia, I-06123 Perugia, Italy*
[45a]*INFN Sezione di Pisa, I-56127 Pisa, Italy*
[45b]*Dipartimento di Fisica, Università di Pisa, I-56127 Pisa, Italy*
[45c]*Scuola Normale Superiore di Pisa, I-56127 Pisa, Italy*
[46]*Princeton University, Princeton, New Jersey 08544, USA*
[47a]*INFN Sezione di Roma, I-00185 Roma, Italy*
[47b]*Dipartimento di Fisica, Università di Roma La Sapienza, I-00185 Roma, Italy*
[48]*Universität Rostock, D-18051 Rostock, Germany*
[49]*Rutherford Appleton Laboratory, Chilton, Didcot, Oxon OX11 0QX, United Kingdom*
[50]*CEA, Irfu, SPP, Centre de Saclay, F-91191 Gif-sur-Yvette, France*
[51]*SLAC National Accelerator Laboratory, Stanford, California 94309 USA*
[52]*University of South Carolina, Columbia, South Carolina 29208, USA*
[53]*Southern Methodist University, Dallas, Texas 75275, USA*
[54]*St. Francis Xavier University, Antigonish, Nova Scotia B2G 2W5, Canada*
[55]*Stanford University, Stanford, California 94305, USA*
[56]*State University of New York, Albany, New York 12222, USA*
[57]*Tel Aviv University, School of Physics and Astronomy, Tel Aviv 69978, Israel*
[58]*University of Tennessee, Knoxville, Tennessee 37996, USA*
[59]*University of Texas at Austin, Austin, Texas 78712, USA*
[60]*University of Texas at Dallas, Richardson, Texas 75083, USA*
[61a]*INFN Sezione di Torino, I-10125 Torino, Italy*

[61b]*Dipartimento di Fisica, Università di Torino, I-10125 Torino, Italy*
[62]*INFN Sezione di Trieste and Dipartimento di Fisica, Università di Trieste, I-34127 Trieste, Italy*
[63]*IFIC, Universitat de Valencia-CSIC, E-46071 Valencia, Spain*
[64a]*Institute of Particle Physics, Victoria, British Columbia V8W 3P6, Canada*
[64b]*University of Victoria, Victoria, British Columbia V8W 3P6, Canada*
[65]*Department of Physics, University of Warwick, Coventry CV4 7AL, United Kingdom*
[66]*University of Wisconsin, Madison, Wisconsin 53706, USA*

(Received 26 August 2018; published 5 December 2018)

We study the process $e^+e^- \to e^+e^-\eta'$ in the double-tag mode and measure for the first time the $\gamma^\star\gamma^\star \to \eta'$ transition form factor $F_{\eta'}(Q_1^2, Q_2^2)$ in the momentum-transfer range $2 < Q_1^2,\ Q_2^2 < 60\ \mathrm{GeV}^2$. The analysis is based on a data sample corresponding to an integrated luminosity of around 469 fb^{-1} collected at the PEP-II e^+e^- collider with the *BABAR* detector at center-of-mass energies near 10.6 GeV.

DOI: 10.1103/PhysRevD.98.112002

I. INTRODUCTION

In this article, we report on the measurement of the $\gamma^\star\gamma^\star \to \eta'$ transition form factor (TFF) by using the two-photon-fusion reaction

$$e^+e^- \to e^+e^-\eta'$$

illustrated by the diagram in Fig. 1. The TFF is defined via the amplitude for the $\gamma^\star\gamma^\star \to \eta'$ transition

$$T = -i4\pi\alpha\epsilon_{\mu\nu\beta\gamma}\varepsilon_1^\mu\varepsilon_2^\nu q_1^\beta q_2^\gamma F_{\eta'}(Q_1^2, Q_2^2), \tag{1}$$

where α is the fine structure constant, $\epsilon_{\mu\nu\alpha\beta}$ is the totally antisymmetric Levi-Civita tensor, $\varepsilon_{1,2}$ and $q_{1,2}$ are the polarization vectors and four-momenta, respectively, of the spacelike photons, $Q_{1,2}^2 = -q_{1,2}^2$, and $F_{\eta'}(Q_1^2, Q_2^2)$ is the transition form factor.

We measure the differential cross section of the process $e^+e^- \to e^+e^-\eta'$ in the double-tag mode, in which both scattered electrons[1] are detected (tagged). The tagged electrons emit highly off-shell photons with momentum transfers $q_{e^+}^2 = -Q_{e^+}^2 = (p_{e^+} - p'_{e^+})^2$ and $q_{e^-}^2 = -Q_{e^-}^2 = (p_{e^-} - p'_{e^-})^2$, where $p_{e^\pm}$ and $p'_{e^\pm}$ are the four-momenta, respectively, of the initial- and final-state electrons. We measure for the first time $F_{\eta'}(Q_1^2, Q_2^2)$ in the kinematic region with two highly off-shell photons $2 < Q_1^2,\ Q_2^2 < 60\ \mathrm{GeV}^2$. The η' transition form factor $F_{\eta'}(Q^2, 0)$ in the spacelike momentum transfer region and in the single-tag mode was measured in several previous experiments [1–5]. The most precise data at large Q^2 were obtained by the CLEO [4] experiment, and then by the *BABAR* [5] experiment, in the momentum transfer ranges $1.5 < Q^2 < 30\ \mathrm{GeV}^2$ and $4 < Q^2 < 40\ \mathrm{GeV}^2$, respectively.

Many theoretical models exist for the description of the TFFs of pseudoscalar mesons, $F_P(Q_1^2, 0)$ and $F_P(Q_1^2, Q_2^2)$ (see e.g., Refs. [6–9]). Measurement of the TFF at large Q_1^2 and Q_2^2 allows the predictions of models inspired by perturbative QCD (pQCD) to be distinguished from those of the vector dominance model (VDM) [10–12]. The tree-level diagrams for VDM and pQCD approaches are shown in Fig. 2. In the case of only one off-shell photon, both classes of models predict the same asymptotic dependence $F_P(Q^2, 0) \sim 1/Q^2$ as $Q^2 \to \infty$, while for two off-shell photons the asymptotic predictions are quite different, $F(Q_1^2, Q_2^2) \sim 1/(Q_1^2 + Q_2^2)$ for pQCD, and $F(Q_1^2, Q_2^2) \sim 1/(Q_1^2 Q_2^2)$ for the VDM model.

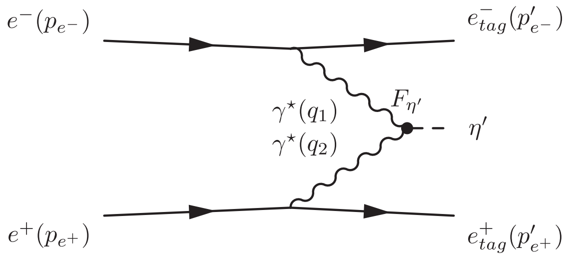

FIG. 1. The diagram for the $e^+e^- \to e^+e^-\eta'$ process.

---

[*] Deceased.
[†] Present address: Wuhan University, Wuhan 430072, China.
[‡] Present address: Università di Bologna and INFN Sezione di Bologna, I-47921 Rimini, Italy.
[§] Present address: University of Huddersfield, Huddersfield HD1 3DH, United Kingdom.
[¶] Present address: University of South Alabama, Mobile, Alabama 36688, USA.
[**] Also at Università di Sassari, I-07100 Sassari, Italy.
[1] Unless otherwise specified, we use the term electron for either an electron or a positron.

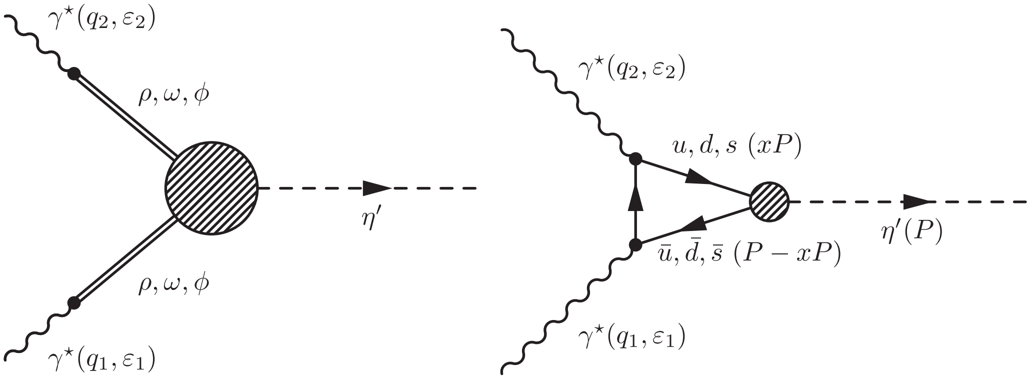

(a) (b)

FIG. 2. The Feynman diagrams for the process $\gamma^\star\gamma^\star \to \eta'$ in the VDM (a) and pQCD (b).

II. THEORETICAL APPROACH TO THE FORM FACTOR $F_{\eta'}(Q_1^2,Q_2^2)$

As a consequence of $\eta - \eta'$ mixing, the η' wave function can be represented as the superposition of two quark-flavor states [13],

$$|\eta'\rangle = \sin\phi|n\rangle + \cos\phi|s\rangle, \tag{2}$$

where

$$|n\rangle = \frac{1}{\sqrt{2}}(|\bar{u}u\rangle + |\bar{d}d\rangle), \qquad |s\rangle = |\bar{s}s\rangle. \tag{3}$$

For the mixing angle ϕ we use the value $\phi = (37.7 \pm 0.7)^\circ$ [14]. The η' transition form factor is related to the form factors for the $|n\rangle$ and $|s\rangle$ states through

$$F_{\eta'} = \sin\phi F_n + \cos\phi F_s. \tag{4}$$

For large values of momentum transfer, pQCD predicts that the form factors F_n and F_s can be represented as a convolution of a hard scattering amplitude T_H and a nonperturbative meson distribution amplitude (DA) $\phi_{n,s}$,

$$F_{n,s}(Q_1^2,Q_2^2) = \int_0^1 T_H(x,Q_1^2,Q_2^2,\mu)\phi_{n,s}(x,\mu)dx, \tag{5}$$

where x is the longitudinal momentum fraction of the quark struck by the virtual photon in the hard scattering process. For the renormalization scale μ, we take $\mu^2 = Q^2 = Q_1^2 + Q_2^2$ as proposed in Ref. [15] and for its asymptotic form $\phi_{n,s}$ [16],

$$\phi_{n,s} = 2C_{n,s}f_{n,s}6x(1-x)(1 + O(\Lambda_{\mathrm{QCD}}^2/\mu^2)), \tag{6}$$

where the charge factors are $C_n = 5/(9\sqrt{2})$ and $C_s = 1/9$, the weak decay constants for the $|n\rangle$ and $|s\rangle$ states are $f_n = (1.08 \pm 0.04)f_\pi$ and $f_s = (1.25 \pm 0.08)f_\pi$ [14], $f_\pi = 130.4 \pm 0.2$ MeV is the pion decay constant, and Λ_{QCD} is the QCD scale parameter.

In the case of two highly off-shell photons, $T_H(x,Q_1^2,Q_2^2)$ can be represented as

$$T_H(x,Q_1^2,Q_2^2) = \frac{1}{2}\frac{1}{xQ_1^2 + (1-x)Q_2^2} \tag{7}$$

$$\cdot\left(1 + C_F\frac{\alpha_s(\mu^2)}{2\pi}t(x,Q_1^2,Q_2^2)\right) + (x \to 1-x) \tag{8}$$

$$+O(\alpha_s^2) + O(\Lambda_{\mathrm{QCD}}^4/Q^4), \tag{9}$$

where $(x \to 1-x)$ stands for the first term with replacement of x by $1-x$, $\alpha_s(\mu^2)$ is the QCD coupling strength, and $C_F = (n_c^2 - 1)/(2n_c) = 4/3$ is a color factor. The expression for the next-to-leading order (NLO) component $t(x,Q_1^2,Q_2^2)$ can be found in Ref. [15], while the leading-order (LO) expression corresponds to $t(x,Q_1^2,Q_2^2) = 0$. Combining Eqs. (4)–(7) we obtain the pQCD prediction for $F_{\eta'}(Q_1^2,Q_2^2)$ at large Q_1^2 and Q_2^2,

$$F_{\eta'}(Q_1^2,Q_2^2) = \left(\frac{5\sqrt{2}}{9}f_n\sin\phi + \frac{2}{9}f_s\cos\phi\right)\int_0^1 dx\frac{1}{2}\frac{6x(1-x)}{xQ_1^2 + (1-x)Q_2^2}\left(1 + C_F\frac{\alpha_s(\mu^2)}{2\pi}t(x,Q_1^2,Q_2^2)\right) + (x \to 1-x). \tag{10}$$

Significant effort has been invested to determine the DAs of pseudoscalar mesons at intermediate values of momentum transfer [15–19]. In contrast to the case of one off-shell photon, the TFF for two off-shell photons is almost insensitive to the shape of the DA, because the amplitude Eq. (7) is finite at the end points $x = 0$ and $x = 1$.

According to the VDM model the TFF for the case of two off-shell photons is

$$F_{\eta'}(Q_1^2, Q_2^2) = \frac{F_{\eta'}(0,0)}{(1 + Q_1^2/\Lambda_P^2)(1 + Q_2^2/\Lambda_P^2)}, \quad (11)$$

where Λ_P is the pole mass parameter (see e.g., Ref. [11]). In the case of the η' meson, Λ_P is found to be $849 \pm 6\ \mathrm{MeV}/c^2$ from the approximation of $F_{\eta'}(Q^2, 0)$ with one off-shell photon [14]. The value of $F_{\eta'}(0,0)$ can be obtained from the measured value of the η' two-photon width $\Gamma_{\eta' \to 2\gamma} = 4.30 \pm 0.16$ keV [20] using the formula [16]

$$F(0,0) = \sqrt{\frac{4\Gamma_{\eta' \to 2\gamma}}{\pi \alpha^2 m_{\eta'}^3}} = 0.342 \pm 0.006\ \mathrm{GeV}^{-1}. \quad (12)$$

III. THE *BABAR* DETECTOR AND DATA SET

The data used in this analysis were collected with the *BABAR* detector at the PEP-II2 asymmetric-energy e^+e^- collider, at the SLAC National Accelerator Laboratory. A total integrated luminosity of 468.6 fb^{-1} [21] is used, including 424.7 fb^{-1} collected at the peak of $\Upsilon(4S)$ resonance and 43.9 fb^{-1} collected 40 MeV below the resonance.

The *BABAR* detector is described in detail elsewhere [22,23]. Charged particles are reconstructed using a tracking system, which includes a silicon vertex tracker (SVT) and a drift chamber (DCH) inside a 1.5 T axial magnetic field. Separation of pions and kaons is accomplished by means of the detector of internally reflected Cherenkov light and energy loss measurements in the SVT and DCH. Photons are detected in the electromagnetic calorimeter (EMC). Muon identification is provided by the instrumented flux return.

Signal $e^+e^- \to e^+e^-\eta'$ events are simulated with the Monte Carlo (MC) event generator GGResRc [24]. Because the $Q^2_{e^-}$, $Q^2_{e^+}$ distributions are peaked near 0, MC events are generated with the requirement $Q^2_{e^-}(Q^2_{e^+}) > 2\ \mathrm{GeV}^2$. This restriction corresponds to the limit of detector acceptance for the tagged electrons. The transition form factor in simulation is assumed to be constant. The GGResRc event generator includes next-to-leading-order radiative corrections to the Born cross section calculated according to Ref. [25]. In particular, it generates extra soft photons emitted by the initial- and final-state electrons. The maximum center-of-mass (c.m.) energy of the photon emitted from the initial state is required to be less than $0.05\sqrt{s}$, where $\sqrt{s}$ is the e^+e^- c.m. energy.

IV. EVENT SELECTION

The decay chain $\eta' \to \pi^+\pi^-\eta \to \pi^+\pi^-2\gamma$ is used to reconstruct the η' meson candidate.

An initial sample of events with at least four tracks and two photon candidates is selected. Tracks must have a point of closest approach to the nominal interaction point that is within 2.5 cm along the beam axis and less than 1.5 cm in the transverse plane. The track transverse momenta must be greater than $50\ \mathrm{MeV}/c$. Electrons and pions are separated using a particle identification (PID) algorithm based on information from the Cherenkov detector, EMC, and the tracking system. An event is required to contain two electron and two pion candidates. The electron PID efficiency is better than 98%, with the pion misidentification probability below 10%. The pion PID efficiency is 98%, with an electron misidentification probability of about 7%.

To recover electron energy loss due to bremsstrahlung, the energy of all the calorimeter showers close to the electron direction (within 35 and 50 mrad for the polar and azimuthal angle, respectively) is combined with the measured energy of the electron track. The resulting c.m. energy of the electron candidate must be greater than 0.2 GeV.

The photon candidates are required to have an energy in the laboratory frame greater than 30 MeV. Two photon candidates are combined to form an η candidate. Their invariant mass is required to be in the 0.45–0.65 GeV/c^2 range. We apply a kinematic fit to the two photons, with an η mass constraint to improve the precision of their momentum measurement. An η' candidate is formed from a pair of oppositely charged pion candidates and an η candidate. The η' candidate invariant mass must be in the range of 0.90–1.02 GeV/c^2.

The final selection uses tagged electrons and is based on variables in the c.m. frame of the initial e^+ and e^-. The total momentum of the reconstructed $e^+e^-\eta'$ system ($P^{\star}_{e^+e^-\eta'}$[2]) must be less than $0.35\ \mathrm{GeV}/c$. The distribution of the total momentum is shown in Fig. 3 for data and simulated signal events. The total energy of the $e^+e^-\eta'$ system must be in the range of 10.30–10.65 GeV as indicated by the arrows in Fig. 4. To reject background from QED events, requirements on the energies of the detected electron and positron are applied. The two-dimensional distributions of the electron c.m. energy versus the positron c.m. energy are shown in Fig. 5 for data and simulated signal events. The lines indicate the boundary of the selection area. Events that lie above and to the right of the lines are rejected.

---

[2] The superscript asterisk indicates a quantity calculated in the e^+e^- c.m. frame.

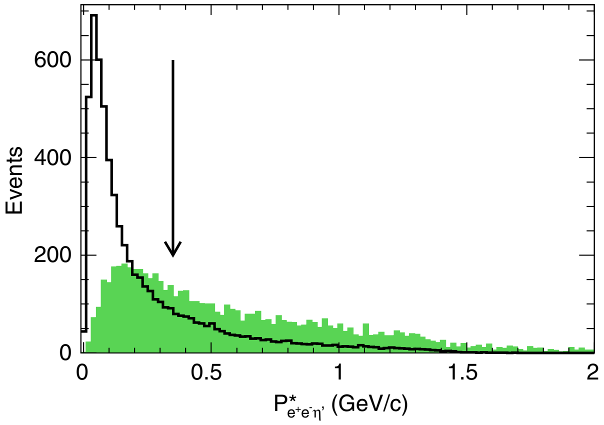

FIG. 3. Distribution of the total momentum of the $e^+e^-\eta'$ system in the c.m. frame. The filled histogram shows the data. The open histogram represents MC simulation normalized to the number of events in data. Events with $P^{\star}_{e^+e^-\eta'} < 0.35$ GeV$/c$ (indicated by the arrow) are retained for further analysis.

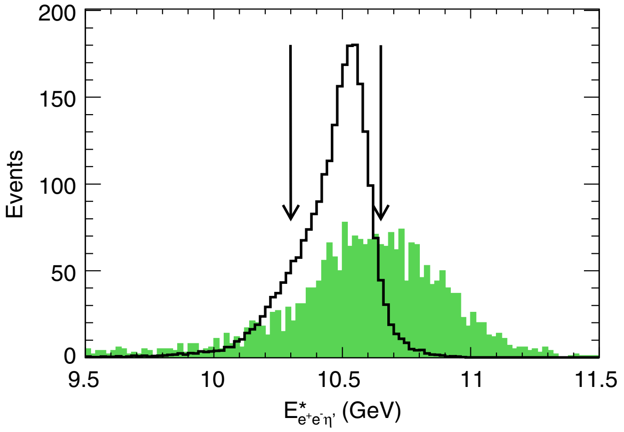

FIG. 4. Distribution of the total energy of the $e^+e^-\eta'$ system in the c.m. frame. The filled histogram shows the data. The open histogram represents MC simulation normalized to the number of events in data. The arrows indicate the boundaries of the region used to select event candidates.

The distribution of the η candidate mass versus the η' one for the selected data and simulated signal samples is shown in Fig. 6. A clustering of events in the central region of the data distribution corresponds to the two-photon η' production. To further suppress background we require that the invariant mass of the η candidate be in the range 0.50–0.58 GeV$/c^2$, as shown by the horizontal lines in Fig. 6. For events with more than one η' or $e^{\pm}$ candidate (about 10% of the selected events), the candidate with smallest absolute value of the total momentum of the $e^+e^-\eta'$ system in the c.m. frame is selected.

Data events that pass all selection criteria are divided into five ($Q^2_{e^-}$, $Q^2_{e^+}$) regions, as illustrated on Fig. 7 for events with $0.945 < M_{\pi^+\pi^-\eta} < 0.972$ GeV/c^2. Because of the symmetry of the process under the exchange of the e^- with the e^+, regions 3 and 4 each include two disjunct regions, mirror symmetric with respect to the diagonal. The number of signal events (N_{events}) in each ($Q^2_{e^-}$, $Q^2_{e^+}$) region is obtained from a fit to the $\pi^+\pi^-\eta$ invariant mass spectrum with a sum of signal and background distributions as shown in Fig. 8. The signal line shape is obtained from the signal simulation, while the background is assumed to be linear. The fitted numbers of events for the five ($Q^2_{e^-}$, $Q^2_{e^+}$) regions are listed in Table I. The total number of signal events is $46.2^{+8.3}_{-7.0}$. For regions 2 and 5 we also use conservative estimates of the number of signal events as upper limits at 90% C.L. using the Feldman-Cousins approach [26].

To estimate the uncertainty related to the description of the background, we repeat the fits using a quadratic background shape. The deviation in the fitted number of signal events is 1.7%. The uncertainty associated with the signal shape (3.3%) is estimated by including in the signal

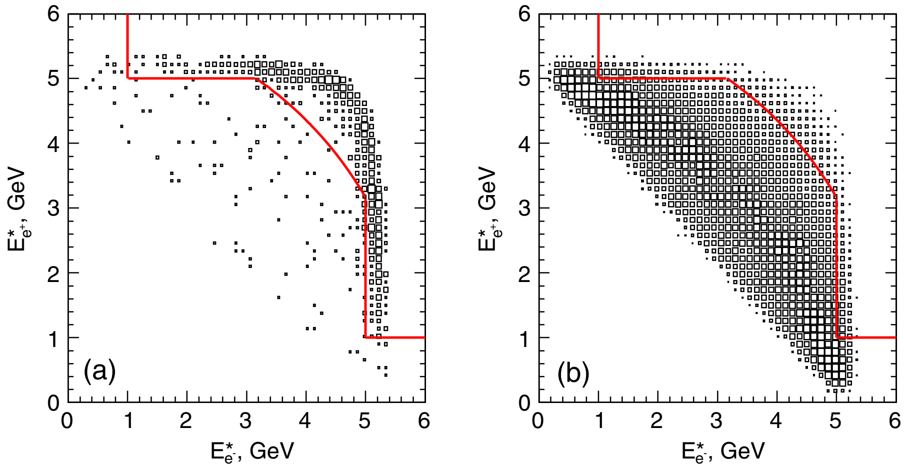

FIG. 5. Distribution of the positron c.m. energy versus the electron c.m. energy for data (a) and simulated signal events (b). The lines indicate the boundary of the selection area. Events that lie above and to the right of the lines are rejected.

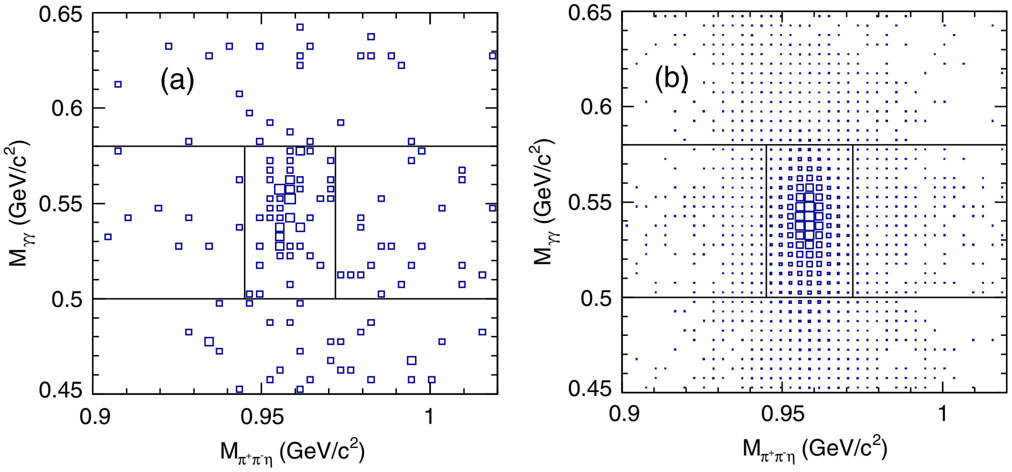

FIG. 6. Distribution of the η candidate mass ($M_{\gamma\gamma}$) versus the η' candidate mass ($M_{\pi^+\pi^-\eta}$) for data (a) and signal MC simulation (b). The horizontal lines indicate the boundaries of the selection condition applied. The vertical lines correspond to the restriction $0.945 < M_{\pi^+\pi^-\eta} < 0.972\ \mathrm{GeV}/c^2$ that is used for the plot of $Q^2_{e^-}$ versus $Q^2_{e^+}$ distribution in Fig. 7.

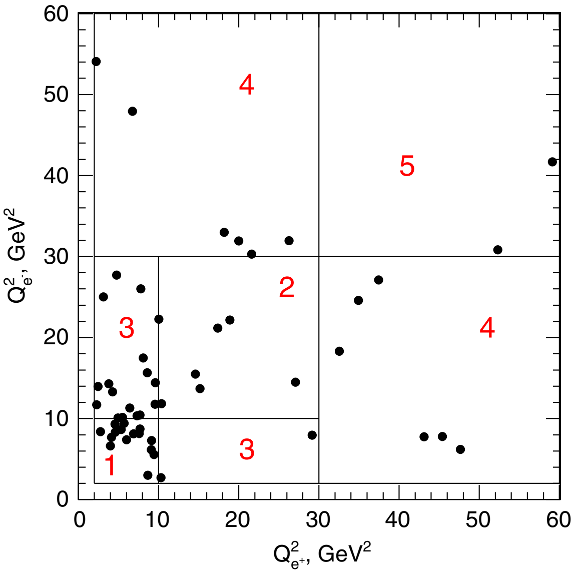

FIG. 7. The $Q^2_{e^-}$ versus $Q^2_{e^+}$ distribution for data events. The lines and numbers indicate the five regions used for the study of the dynamics of TFF a function of $Q^2_{e^-}$ and $Q^2_{e^+}$.

probability function a mass shift $\Delta M_{\pi^+\pi^-\eta} = -0.48\ \mathrm{MeV/c^2}$ and additional Gaussian smearing width $\sigma(M_{\pi^+\pi^-\eta}) = 1\ \mathrm{MeV}/c^2$. These parameters are obtained from our previous study of $\gamma\gamma^* \to \eta'$ events [5], based on single-tagged events, where the statistical precision was significantly larger. The total systematic uncertainty (3.7%) is obtained by adding the individual terms in quadrature.

Following the methods developed in the single-tag analysis of Ref. [5], we have studied possible sources of peaking background: e^+e^- annihilation into hadrons, the two-photon process $e^+e^- \to e^+e^-\eta'\pi^0$, and the vector meson bremsstrahlung processes $e^+e^- \to e^+e^-\phi \to e^+e^-\eta'\gamma$ and $e^+e^- \to e^+e^-J/\psi \to e^+e^-\eta'\gamma$. As in Ref. [5], the impact of these processes on the results is found to be negligible.

V. DETECTION EFFICIENCY

The detection efficiency (ε) is determined from MC simulation in the ($Q^2_{e^-}$, $Q^2_{e^+}$) plane as the ratio of the selected over generated events and is shown in Fig. 9. The detector acceptance limits the efficiency at small momenta and the minimum measurable Q^2 is 2 GeV^2. The difference between the energies of the e^+ and e^- beams at PEP-II leads to an asymmetry in the dependence of the efficiency on $Q^2_{e^+}$ and $Q^2_{e^-}$.

Because of the symmetry of the form factor $F_{\eta'}(Q_1^2, Q_2^2) = F_{\eta'}(Q_2^2, Q_1^2)$, we use the notation

$$Q_1^2 = \max(Q^2_{e^+}, Q^2_{e^-}), \qquad Q_2^2 = \min(Q^2_{e^+}, Q^2_{e^-}). \tag{13}$$

Since signal MC events are generated with a constant TFF, the average detection efficiency for the specific (Q_1^2, Q_2^2) region is calculated as the ratio of the following integrals:

$$\varepsilon_{\mathrm{true}} = \frac{\int \varepsilon(Q_1^2, Q_2^2) F^2_{\eta'}(Q_1^2, Q_2^2) dQ_1^2 dQ_2^2}{\int F^2_{\eta'}(Q_1^2, Q_2^2) dQ_1^2 dQ_2^2}, \tag{14}$$

where the form factor is described by Eq. (10). The obtained values of the detection efficiency for the five (Q_1^2, Q_2^2) regions are listed in Table I.

The systematic uncertainties related to the detection efficiency are listed in Table II. The uncertainties related to track reconstruction, $\eta \to 2\gamma$ reconstruction, trigger and filters, and the pion PID were studied in our previous single-tag analysis [5]. To estimate the efficiency uncertainty related to other selection criteria, we apply a less

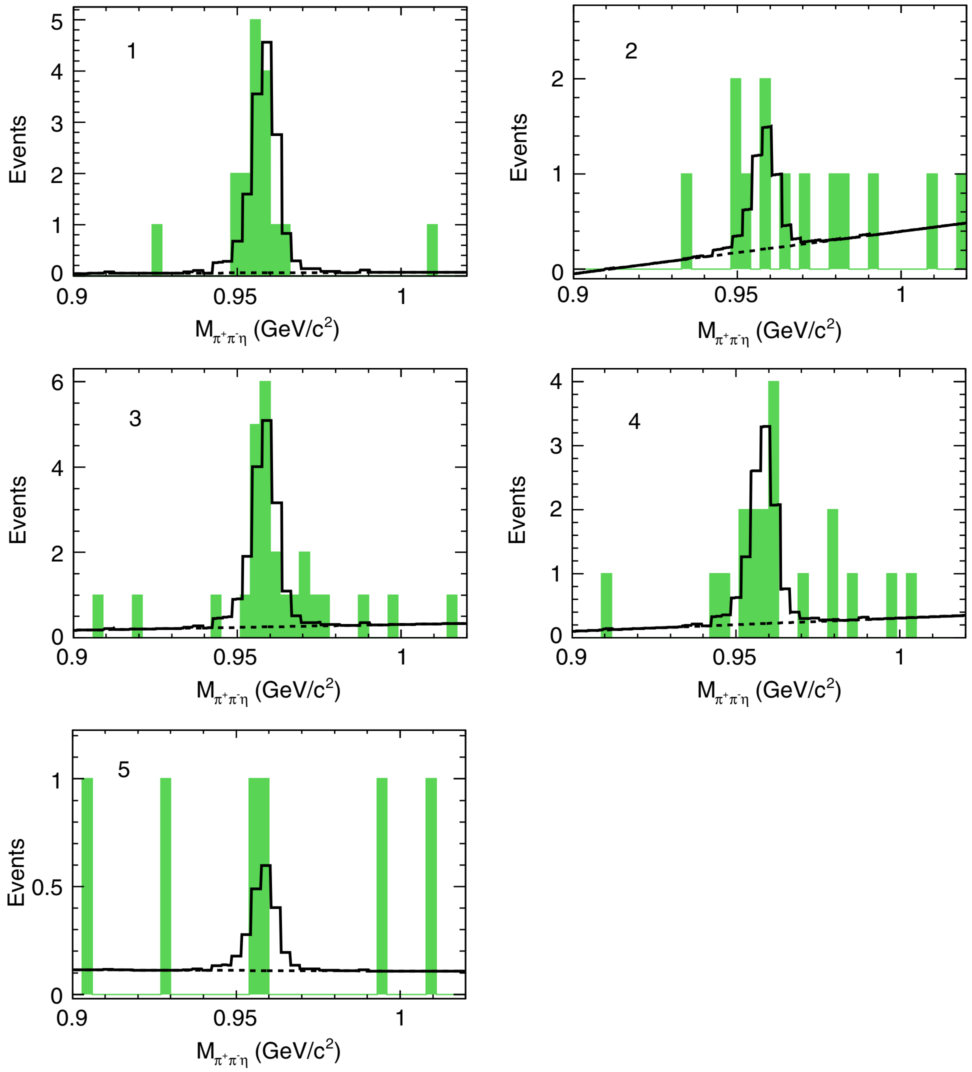

FIG. 8. The $\pi^+\pi^-\eta$ mass spectra for data events from the five (Q_1^2, Q_2^2) regions of Fig. 7. The open histograms are the fit results. The dashed lines represent fitted background.

TABLE I. The weighted averages $\overline{Q_1^2}$ and $\overline{Q_2^2}$ for the (Q_1^2, Q_2^2) region, the boundaries of the (Q_1^2, Q_2^2) region, the detection efficiency ($\varepsilon_{\text{true}}$), the radiative correction factor (R), the number of selected signal events (N_{events}), the cross section ($d^2\sigma(\overline{Q_1^2}, \overline{Q_2^2})/(dQ_1^2 dQ_2^2)$) with its statistical uncertainty, and the $\gamma^\star\gamma^\star \to \eta'$ transition form factor ($F(\overline{Q_1^2}, \overline{Q_2^2})$) with the statistical, systematic, and model uncertainties (see the text). All presented upper limits correspond to 90% C.L.

$\overline{Q_1^2}, \overline{Q_2^2}$ (GeV^2)	(Q_1^2, Q_2^2) region (GeV^2)	$\varepsilon_{\text{true}}$	R	N_{events}	$d^2\sigma/(dQ_1^2 dQ_2^2)$ $\times 10^4$ (fb/GeV^4)	$F(\overline{Q_1^2}, \overline{Q_2^2})$ $\times 10^3$ (GeV^{-1})
6.48, 6.48	$2 < Q_1^2, Q_2^2 < 10$	0.019	1.03	$14.7^{+4.3}_{-3.6}$	$1471.8^{+430.1}_{-362.9}$	$14.32^{+1.95}_{-1.89} \pm 0.83 \pm 0.14$
16.85, 16.85	$10 < Q_1^2, Q_2^2 < 30$	0.282	1.10	$4.2^{+3.1}_{-2.7}$	$4.2^{+3.1}_{-2.7}$	$5.35^{+1.71}_{-2.15} \pm 0.31 \pm 0.42$
				< 9	< 9	< 13
14.83, 4.27	$10 < Q_1^2 < 30; 2 < Q_2^2 < 10$	0.145	1.07	$15.8^{+4.8}_{-4.0}$	$39.7^{+12.0}_{-10.2}$	$8.24^{+1.16}_{-1.13} \pm 0.48 \pm 0.65$
38.11, 14.95	$30 < Q_1^2 < 60; 2 < Q_2^2 < 30$	0.226	1.11	$10.0^{+3.9}_{-3.2}$	$3.0^{+1.2}_{-1.0}$	$6.07^{+1.09}_{-1.07} \pm 0.35 \pm 1.21$
45.63, 45.63	$30 < Q_1^2, Q_2^2 < 60$	0.293	1.22	$1.6^{+1.8}_{-1.1}$	$0.6^{+0.7}_{-0.4}$	$8.71^{+3.96}_{-4.02} \pm 0.50 \pm 1.04$
				< 4	< 1.5	< 25

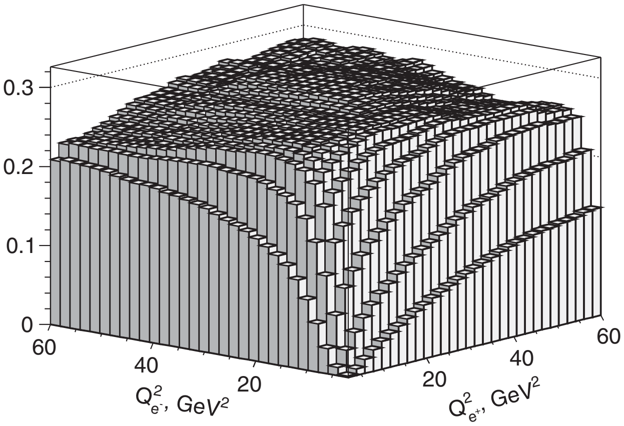

FIG. 9. Detection efficiency as a function of the momentum transfers $Q^2_{e^-}$ and $Q^2_{e^+}$.

strict condition on a criterion, perform the procedure of background subtraction described in the previous section, and calculate the ratio of the number of selected events in data and simulation. We consider the less strict requirements $P^\star_{e^+e^-\eta'} < 1$ GeV$/c$, $10.20 < E^\star_{e^+e^-\eta'} < 10.75$ GeV, $0.48 < M_{\gamma\gamma} < 0.60$ GeV$/c^2$, and remove the requirements on E_{e^+} and E_{e^-} entirely. The quadratic sum of the deviations from the nominal value of the ratio (11%) is used as the total systematic uncertainty of the detection efficiency.

VI. CROSS SECTION AND FORM FACTOR

The differential Born cross section for the process $e^+e^- \to e^+e^-\eta'$ is calculated as

$$\frac{d^2\sigma}{dQ_1^2dQ_2^2} = \frac{1}{\varepsilon_{\mathrm{true}}R\mathcal{L}\mathcal{B}}\frac{d^2N}{dQ_1^2dQ_2^2}, \tag{15}$$

where $d^2N/(dQ_1^2dQ_2^2)$ is the number of signal events in the (Q_1^2, Q_2^2) region divided by the area of this region, $\mathcal{L}$ is the integrated luminosity, and R is a radiative correction factor accounting for distortion of the $Q_{1,2}^2$ spectrum due to the emission of photons from the initial state and for vacuum polarization effects. The factor $\mathcal{B}$ is the product of the branching fractions $\mathcal{B}(\eta' \to \pi^+\pi^-\eta)\mathcal{B}(\eta \to \gamma\gamma) = 0.169 \pm 0.003$ [20]. The radiative correction factor R is determined using simulation at the generator level, i.e., without detector simulation. The $Q_{1,2}^2$ spectrum is generated using only the pure Born amplitude for the $e^+e^- \to e^+e^-\eta'$ process, and then using a model with radiative corrections included. The factor R is evaluated as the ratio of the second spectrum to the first. The values of the cross section for the five (Q_1^2, Q_2^2) regions are listed in Table I. The cross section in the entire range of momentum transfer $2 < Q_1^2, Q_2^2 < 60$ GeV^2 is

$$\sigma = 11.4^{+2.8}_{-2.4}\ \mathrm{fb}, \tag{16}$$

TABLE II. The sources of the systematic uncertainties in the $e^+e^- \to e^+e^-\eta'$ cross section.

Source	Uncertainty (%)
$\pi^\pm$ identification	1.0
$e^\pm$ identification	1.0
Other selection criteria	11.0
Track reconstruction	0.9
$\eta \to 2\gamma$ reconstruction	2.0
Trigger, filters	1.3
Background subtraction	3.7
Radiative correction	1.0
Luminosity	1.0
Total	12%

where the uncertainty is statistical. The systematic uncertainty includes the uncertainty in the number of signal events associated with background subtraction (Sec. IV), the uncertainty in the detection efficiency (Sec. V), the uncertainty in the calculation of the radiative correction (1%) [25], and the uncertainty in the integrated luminosity (1%) [21]. All sources of systematic uncertainty in the cross section are summarized in Table II. The total systematic uncertainty (12%) is the sum in quadrature of all the systematic contributions. The model uncertainty is discussed below.

To extract the TFF we compare the value of the measured cross section from Eq. (15) with the calculated one. The latter is evaluated using $F^2_{\eta'}(Q_1^2, Q_2^2)$ obtained from Eq. (10). Therefore, the measured form factor is determined as

$$F^2(\overline{Q_1^2}, \overline{Q_2^2}) = \frac{(d^2\sigma/(dQ_1^2dQ_2^2))_{\mathrm{data}}}{(d^2\sigma/(dQ_1^2dQ_2^2))_{\mathrm{MC}}}F^2_{\eta'}(\overline{Q_1^2}, \overline{Q_2^2}), \tag{17}$$

where $F^2_{\eta'}(\overline{Q_1^2}, \overline{Q_2^2})$ and $(d^2\sigma/(dQ_1^2dQ_2^2))_{\mathrm{MC}}$ correspond to Eq. (10).

The average momentum transfer squared for each (Q_1^2, Q_2^2) region is calculated using the data spectrum normalized to the detection efficiency,

$$\overline{Q_{1,2}^2} = \frac{\sum_i Q_{1,2}^2(i)/\varepsilon(Q_1^2, Q_2^2)}{\sum_i 1/\varepsilon(Q_1^2, Q_2^2)}. \tag{18}$$

For regions 1, 2, and 5, the $\overline{Q_1^2}$ and $\overline{Q_2^2}$ are additionally averaged.

The model uncertainty arises from the model dependence of $(d^2\sigma/(dQ_1^2dQ_2^2))_{\mathrm{MC}}$ and $\varepsilon_{\mathrm{true}}$. Repeating the calculation of Eqs. (14), (15), and (17) with a constant TFF, we estimate the model uncertainty. In the case of the cross section it is about 60% because of the strong dependence of $\varepsilon_{\mathrm{true}}$ on the input model for TFF at small values of Q_1^2 and Q_2^2. However, the transition form factor is much less sensitive to the model.

The obtained values of the transition form factor are listed in Table I and are represented in Fig. 10 by the

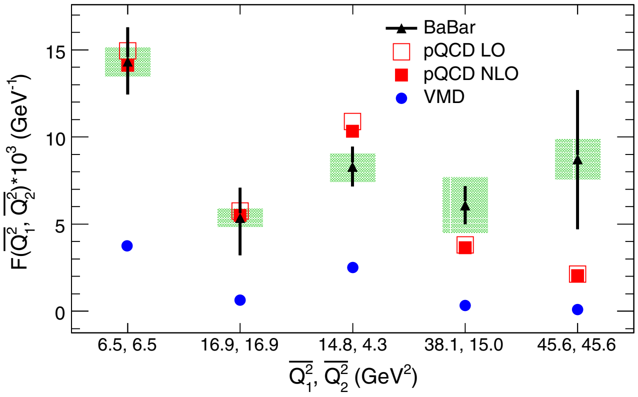

FIG. 10. Comparison of the measured $\gamma^\star\gamma^\star \to \eta'$ transition form factor (triangles, with error bars representing the statistical uncertainties) with the LO (open squares) and NLO (filled squares) pQCD predictions and the VDM predictions (circles).

triangles. The error bars attached to the triangles indicate the statistical uncertainties. The quadratic sum of the systematic and model uncertainties is shown by the shaded rectangles. The open and filled squares in Fig. 10 correspond to the LO and NLO pQCD predictions [Eq. (10)], respectively. The NLO correction is relatively small. The measured TFF is, in general, consistent with the QCD prediction. The circles in Fig. 10 represent the predictions of the VDM model [Eq. (11)], which exhibits a clear disagreement with the data.

VII. SUMMARY

We have studied for the first time the process $e^+e^- \to e^+e^-\eta'$ in the double-tag mode and have measured the $\gamma^\star\gamma^\star \to \eta'$ transition form factor in the momentum-transfer range $2 < Q_1^2, Q_2^2 < 60$ GeV^2. The measured values of the form factor are in agreement with the pQCD prediction and contradict the prediction of the VDM model.

ACKNOWLEDGMENTS

We are grateful for the extraordinary contributions of our PEP-II2 colleagues in achieving the excellent luminosity and machine conditions that have made this work possible. The success of this project also relies critically on the expertise and dedication of the computing organizations that support *BABAR*. The collaborating institutions wish to thank SLAC for its support and the kind hospitality extended to them. This work is supported by the U.S. Department of Energy and National Science Foundation, the Natural Sciences and Engineering Research Council (Canada), the Commissariat à l'Energie Atomique and Institut National de Physique Nucléaire et de Physique des Particules (France), the Bundesministerium für Bildung und Forschung and Deutsche Forschungsgemeinschaft (Germany), the Istituto Nazionale di Fisica Nucleare (Italy), the Foundation for Fundamental Research on Matter (Netherlands), the Research Council of Norway, the Ministry of Education and Science of the Russian Federation, Ministerio de Economía y Competitividad (Spain), the Science and Technology Facilities Council (United Kingdom), and the Binational Science Foundation (U.S.-Israel). Individuals have received support from the Russian Foundation for Basic Research (Grant No. 18-32-01020), the Marie-Curie IEF program (European Union) and the A. P. Sloan Foundation (USA).

---

[1] C. Berger *et al.* (PLUTO Collaboration), Phys. Lett. **142B**, 125 (1984).
[2] H. Aihara *et al.* (TPC/Two Gamma Collaboration), Phys. Rev. D **38**, 1 (1988); Phys. Rev. Lett. **64**, 172 (1990).
[3] H.-J. Behrend *et al.* (CELLO Collaboration), Z. Phys. C **49**, 401 (1991).
[4] J. Gronberg *et al.* (CLEO Collaboration), Phys. Rev. D **57**, 33 (1998).
[5] P. del Amo Sanchez *et al.* (*BABAR* Collaboration), Phys. Rev. D **84**, 052001 (2011).
[6] G. Kopp, T. F. Walsh, and P. M. Zerwas, Nucl. Phys. **B70**, 461 (1974).
[7] S. Berman and D. Geffen, Nuovo Cimento **18**, 1192 (1960).
[8] P. Kroll, Nucl. Phys. B, Proc. Suppl. **219–220**, 2 (2011).
[9] S. Agaev, V. M. Braun, N. Offen, F. A. Porkert, and A. Schäfer, Phys. Rev. D **90**, 074019 (2014).
[10] B.-l. Young, Phys. Rev. **161**, 1620 (1967).
[11] L. G. Landsberg, Phys. Rep. **128**, 301 (1985).
[12] A. Dorokhov, M. Ivanov, and S. Kovalenko, Phys. Lett. B **677**, 145 (2009).
[13] T. Feldmann, P. Kroll, and B. Stech, Phys. Rev. D **58**, 114006 (1998).
[14] F.-G. Cao, Phys. Rev. D **85**, 057501 (2012).
[15] E. Braaten, Phys. Rev. D **28**, 524 (1983).
[16] S. J. Brodsky and G. P. Lepage, Phys. Rev. D **24**, 7 (1981); G. P. Lepage and S. J. Brodsky, Phys. Rev. D **22**, 2157 (1980).
[17] V. L. Chernyak and A. R. Zhitnitsky, Nucl. Phys. **B201**, 492 (1982); Phys. Rep. **112**, 173 (1984); Nucl. Phys. **B246**, 52 (1984).
[18] T. Feldmann and P. Kroll, Phys. Rev. D **58**, 057501 (1998).
[19] A. J. Brodsky, F. Cao, and G. Teramond, Phys. Rev. D **84**, 033001 (2011).
[20] C. Patrignani *et al.* (Particle Data Group), Chin. Phys. C **40**, 100001 (2016).

[21] J. P. Lees *et al.* (*BABAR* Collaboration), Nucl. Instrum. Methods Phys. Res., Sect. A **726**, 203 (2013).

[22] B. Aubert *et al.* (*BABAR* Collaboration), Nucl. Instrum. Methods A **479**, 1 (2002).

[23] B. Aubert *et al.* (*BABAR* Collaboration), Nucl. Instrum. Methods A **729**, 615 (2013).

[24] V. P. Druzhinin, L. V. Kardapoltsev, and V. A. Tayursky, Comput. Phys. Commun. **185**, 236 (2014).

[25] S. Ong and P. Kessler, Phys. Rev. D **38**, 2280 (1988).

[26] G. J. Feldman and R. D. Cousins, Phys. Rev. D **57**, 3873 (1998).